

Angular correlations and internal conversion coefficients of  $\gamma$ -ray transitions in  $^{104}\text{Pd}$ M. E. Bellizzi,<sup>1</sup> A. Giannatiempo,<sup>1,2</sup> A. Nannini,<sup>2</sup> A. Perego,<sup>1,2</sup> and P. Sona<sup>1,2</sup><sup>1</sup>Dipartimento di Fisica, Università di Firenze, Florence, Italy<sup>2</sup>Istituto Nazionale di Fisica Nucleare, Sezione di Firenze, Florence, Italy

(Received 30 November 2000; published 18 May 2001)

The nucleus  $^{104}\text{Pd}$ , populated in the electron capture and  $\beta^+$  decay of  $^{104}\text{Ag}$ , has been investigated by means of  $\gamma$ - $\gamma$  coincidence,  $\gamma$ - $\gamma$  angular correlation, and  $K$  internal conversion coefficient measurements. The results have led to an improved knowledge of the decay scheme, to spin-parity assignment to several levels, and to the determination of  $E2/M1$  mixing ratios for the most intense transitions. Information on  $E0$  transitions between  $0^+$  states and between states of same  $J \neq 0$  has also been deduced. The new spectroscopic data have been used to give an updated version of the decay scheme of  $^{104}\text{Pd}$ .

DOI: 10.1103/PhysRevC.63.064313

PACS number(s): 23.20.Lv, 23.20.Nx, 21.10.Hw, 27.60.+j

## I. INTRODUCTION

Even palladium isotopes belong to a mass region ( $A \approx 100$ ) where nuclei display a transitional character from vibrational to gamma soft. Very recently they have been the object of extensive analyses in the framework of the interacting boson approximation (IBA) model [1] in both its IBA-1 [2] and IBA-2 [3–5] versions. In the latter case special attention has been paid to the identification of states with mixed-symmetry (MS) character in the proton and neutron degrees of freedom [6,7]. The role played by these states in determining the excitation energy patterns at low energy along the isotopic chain has been pointed out in Ref. [4]. The systematic analysis of these isotopes was complicated by the rather fragmentary experimental information. For example, in  $^{102,104}\text{Pd}$  many important spectroscopic data, particularly useful to test the model predictions, such as definite spin-parity assignments or  $E2/M1$  mixing ratios  $\delta$ , were missing.

To extend to  $^{104}\text{Pd}$  the possibility of a stringent comparison between experimental and calculated data we have performed  $\gamma$ - $\gamma$  coincidence,  $\gamma$ - $\gamma$  angular correlation, and  $K$ -internal conversion coefficient measurements in this isotope, populated through the electron capture (EC) and  $\beta^+$  decay of the  $5^+$  ground state and  $2^+$  metastable state of  $^{104}\text{Ag}$ .

The experimental setup for angular correlation measurements as well as the procedure followed to deduce spins and  $\delta$  values are described in Sec. II A. Section II B is dedicated to the results, obtained from electron-conversion measurements, on the multiplicities and the absolute values of mixing ratios of several transitions as well as on  $E0$  components in  $\Delta J=0$  transitions. The body of experimental information obtained is used in Sec. II C to provide an updated version of the decay scheme of  $^{104}\text{Pd}$ .

## II. EXPERIMENTAL PROCEDURE AND RESULTS

Levels of  $^{104}\text{Pd}$  were populated in the EC- $\beta^+$  decay of  $^{104g}\text{Ag}$  ( $T_{1/2}=69$  min) and  $^{104m}\text{Ag}$  ( $T_{1/2}=34$  min) produced via ( $p,n$ ) reaction on a target of  $^{104}\text{Pd}$  (99% enriched). The target,  $\sim 1$  mg/cm<sup>2</sup> thick, was obtained by vacuum deposition of the isotope on a 0.3 mm thick aluminum backing. A proton beam of 6.8 MeV energy was used with a typical

current of  $\sim 1$   $\mu\text{A}$ . Energy spectra  $\gamma$  rays were recorded up to an energy of 2.7 MeV in  $\gamma$ - $\gamma$  coincidence measurements and up to an energy of 3.5 MeV in electron-conversion measurements.

A.  $\gamma$ - $\gamma$  coincidence and angular correlation measurements

An apparatus where the irradiation site was separated from the counting one was utilized for  $\gamma$ - $\gamma$  measurements. The target could be shifted vertically, by means of a rack, over a distance of 20 cm (see Fig. 1) while maintaining the

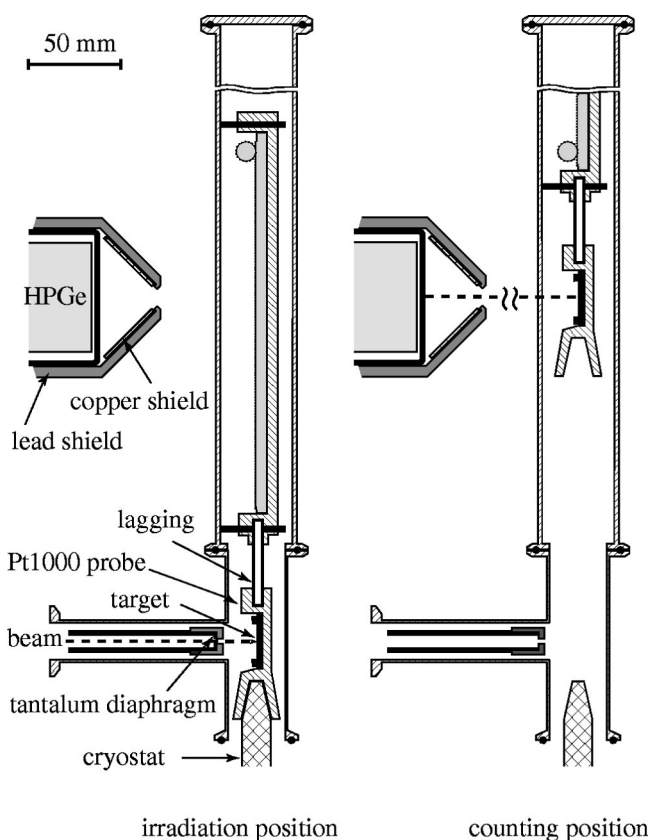


FIG. 1. Schematic view of the target chamber utilized in the angular correlation measurements. The target can be shifted vertically, while maintaining the vacuum in the chamber.

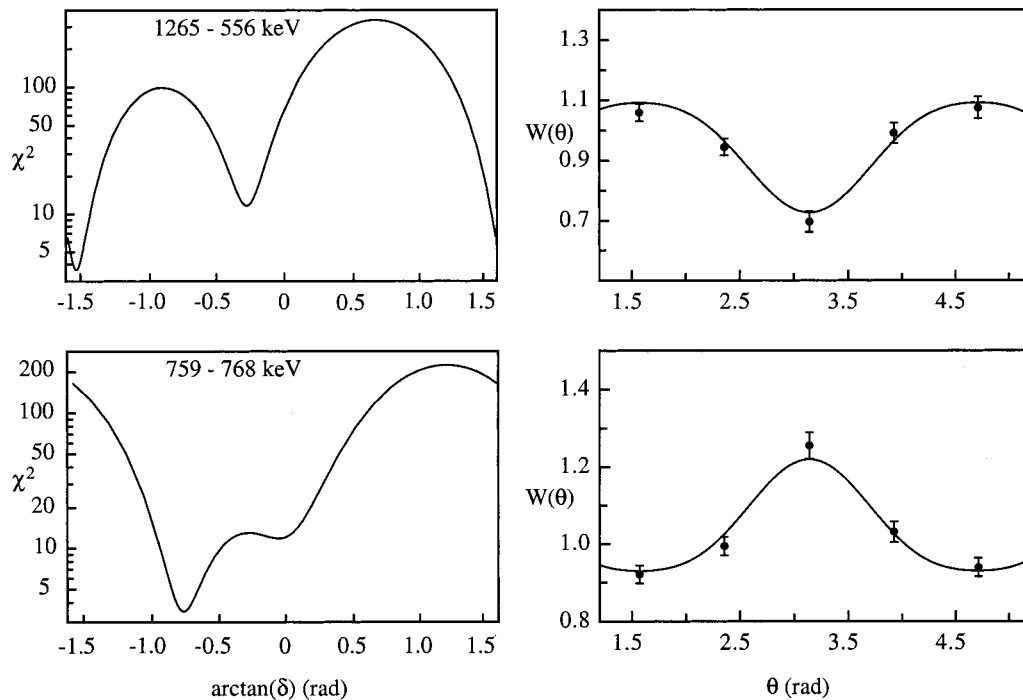


FIG. 2. Angular correlation plots of the indicated transitions in  $^{104}\text{Pd}$ . On the left, plots of  $\chi^2$  versus  $\arctan(\delta)$  for the upper transition in the cascade indicated in each panel. On the right, the angular correlation function corresponding to the minimum  $\chi^2$  value of  $\delta$  is plotted together with the experimental points.

vacuum in the target chamber. At the irradiation site the target was in thermal contact with a cold finger (cooled down to liquid nitrogen temperature) to avoid possible damage due to the high power load. The upper position of the target (source) was at the center of a circular rail where three braces supporting three coaxial high-purity (HP) Ge detectors (120 cm<sup>3</sup> active volume each) could be rotated over the whole  $2\pi$  range, at an adjustable distance from the target (7 cm in the present work). The detectors had a typical energy resolution of 2.3 keV [full width at half maximum (FWHM)] at 1.33 MeV  $\gamma$ -ray energy and 25% relative efficiency. Cone-shaped lead shields (internally copper-lined) were utilized to define the acceptance of the detectors and to minimize  $\gamma$  cross-scattering effects. Particular care was devoted to obtain a high reproducibility of the target position at the two sites. The beam spot was defined by a tantalum diaphragm (2 mm diameter) located 1 cm upstream of the target. The adopted setup makes it possible to conveniently shield the detectors from the neutrons produced at the irradiation site and to use a closed rail, i.e., without openings for the beam pipe.

The measurements were performed by alternating a 360 s activation time, a 60 s waiting time to reduce the background due to short-lived activities, a 2700 s measuring time, and a 100 s waiting time, sufficient for the target (having reached the bombarding site) to cool down from about  $-50^\circ\text{C}$  to about  $-120^\circ\text{C}$ , as monitored by a thermocouple (see Fig. 1).

Coincidence measurements were performed by keeping a detector fixed and positioning the two mobile detectors at angles of  $90^\circ$ ,  $125^\circ$ ,  $180^\circ$ ,  $225^\circ$ , and  $270^\circ$  relative to the fixed one (the brace of the fixed detector could be lifted so as

to allow the passage of the braces of the movable ones). A typical run in a given geometry lasted about three hours and measurements at each angle were repeated at least three times in a random sequence.

For each coincidence event involving a movable detector and the fixed one, the  $\gamma$ -ray energies and the time interval between the signals from the two detectors were collected and stored on magnetic tape for off-line analysis. The resolving time for a coincidence event was  $\sim 30$  ns (FWHM). Coincidence spectra for each angle  $\theta$  were generated by setting energy gates in the spectrum of the fixed detector. To correct for the contribution of accidental coincidences two gates of the same width were set on the right and on the left of the prompt peak in the time spectrum. To estimate the true-coincidence contribution from the background under each  $\gamma$  peak of interest, two gates of equal width were also set on the continuum on both sides of the gating transition. For each detector pair and each  $\gamma$ - $\gamma$  cascade, the nine energy spectra thereby obtained (including those gated by the prompt peak in the time spectrum and by the full energy peak in the energy spectrum) were properly combined to derive the final coincidence energy spectra. Singles spectra from movable detectors were simultaneously collected at each angle. These were used to correct peak areas in the coincidence spectra to take into account possible differences in the absorption of  $\gamma$  rays at different angles as well as possible effects due to the eccentricity of the circular rail track and changes in the average beam spot position.

To deduce the experimental correlation function  $W(\theta)$ , for each cascade of interest the number of coincidences has been divided by a coefficient obtained by normalizing the coincidence intensities of a known  $E2$ - $E2$  cascade (having

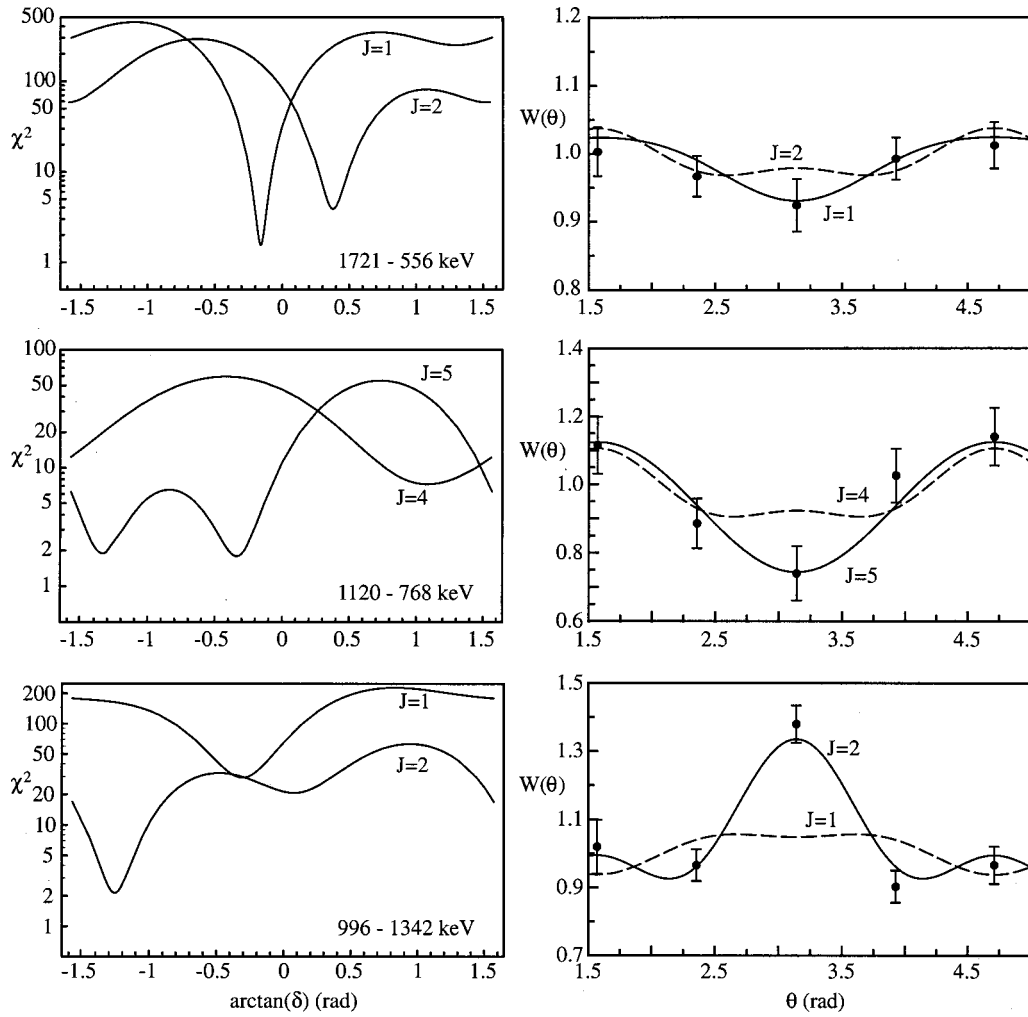


FIG. 3. Angular correlation plots of the indicated transitions in  $^{104}\text{Pd}$ . On the left, plots of  $\chi^2$  versus  $\arctan(\delta)$  for the upper transition in the cascade indicated in each panel. Different curves refer to different hypotheses on the spin value of the uppermost state in the cascade. On the right, the angular correlation function corresponding to the minimum  $\chi^2$  value of  $\delta$  is plotted together with the experimental points. The function corresponding to the selected spin value is reported as a full line, that of the alternative value as a dashed line.

the lower transition in common with the cascade of interest) to the corresponding theoretical correlation function.

For each  $\gamma$ - $\gamma$  cascade two independent sets of values of  $W(\theta)$  have been deduced, corresponding to the two mobile detectors; the weighted average was then taken to obtain a single angular correlation function. In all  $\gamma$ - $\gamma$  cascades considered in the angular correlation analysis, the lower transition has a pure  $E2$  multipolarity, so that only the mixing ratio of the upper transition and, in some cases, the spin of the upper level are unknown.

To evaluate the mixing ratio of the upper transition when the spin sequence of the cascade of interest was known, a minimum  $\chi^2$  procedure has been adopted, based on a fit to the correlation function

$$W(\theta) = 1 + Q_{22}A_{22}(\delta)P_2(\cos\theta) + Q_{44}A_{44}(\delta)P_4(\cos\theta).$$

Here  $Q_{kk}$  are the attenuation factors and  $A_{kk}$  are given as a function of  $\delta$ , according to the Krane-Steffen [8] phase convention. The values of  $Q_{kk}$  have been numerically evaluated following Ref. [9].

When the spin of the upper level was unknown, the same procedure was repeated for each spin value compatible with the information previously available and the constraints derived in the present work (see Sec. II C).

Typical angular correlation plots are shown on the right-hand side of Figs. 2 and 3 and the corresponding plots of  $\chi^2$  versus  $\arctan(\delta)$  are plotted on the left-hand side. The results of the present work are summarized in Table I. The quoted uncertainties on the mixing ratios correspond to the intersection of the function  $\chi^2(\arctan(\delta))$  with the line  $\chi^2 = \chi^2_{\min} + 1$ .

In the particular case of the level at 2276 keV, for which it has been possible to measure angular correlations for two different deexciting cascades, the overall likelihood ratio (higher than 5 to 1) favors the  $J=1$  hypothesis with respect to the  $J=2$  one, so that the assignment  $J=1$  is clearly to be preferred.

The assignment  $J=4$  to the 2571 keV levels has also been based on the likelihood ratio.

The comparison with previously measured values of  $\delta$  (also given in Table I) shows good agreement in three cases

TABLE I. Data relevant to the  $\gamma$ - $\gamma$  angular correlation measurements in  $^{104}\text{Pd}$ . In the first three columns are given the quantities that identify the cascades, as taken from Ref. [16]. In the fourth and fifth columns are reported the spin values of the initial level in the cascade and the  $E2/M1$  mixing ratios obtained in the present work. In the sixth column are shown the  $\delta$  values from previous work [10]. For  $\gamma$  transitions from levels having two possible spin assignments the two corresponding values of  $\delta$  are reported.

Level (keV)	Cascade	$J$ sequence	$J_i$	$\delta$ (this work)	$\delta$ [10]
1342	786–556	2–2–0		$-32_{-170}^{+16}$	-4.8(42)
1794	1238–556	2–2–0		+0.14(9)	
1821	1265–556	3–2–0		$-15_{23}^{+6}$	0.23(7) or $ \delta  > 13$
2082	759–768	4–4–2		-0.90(14)	-0.84(24)
2182	858–768	4–4–2		+0.05(10)	0.45(30)
2244	1689–556	2–2–0		-0.13(7)	
2265	942–768	4–4–2		-3.5(8)	-0.64(14) or 5.0(23)
2276	1721–556	1,2–2–0	1	-0.16(3)	
	935–1342	1,2–2–0	1	-0.14(7)	
2338	996–1342	1,2–2–0	2	-3.1(9)	
2444	1120–768	4,5,6–4–2	5	$-0.35(15)$ or $-3.9_{-4.7}^{+1.7}$	
2533	1977–556	(1,2,3)–2–0	2	-5(2)	
2571	1247–768	-4–2	4	-0.86(7)	
2695	2139–556	2–2–0		-0.11(6)	
2774	1451–768	4–4–2		$-0.9_{0.3}^{+1.0}$	
2868	1545–768	-4–2	(4)	-0.90(13)	
2924	1600–768	(4,5,6)–4–2	4, 5	-0.5(6), 0.8(14)	
2975	2420–556	(1,2,3)–2–0	2, 3	0.07(7), 0.4(2)	
3078	2522–556	2,3–2–0	2, 3	-2.1(5), 0.6(4)	
3105	1782–768	4–4–2		0.24(10) or -1.4(3)	
3113	863–926	5,6–6–4	5, 6	-0.50(8), -0.28(8)	
3137	1814–768	4–4–2		-0.5(4)	
3158	908–926	4–6–4	5, 6	-0.25(6), 0.34(9)	
3183	2627–556	-2–0	2, 3	-0.11(9), 0.8(4)	
3310	1986–768	4,5,6–4–2	4	-1.4(6)	

while our value for  $\delta(3_1^+ \rightarrow 2_1^+; 1265 \text{ keV})$  is only consistent with the upper limit of Ref. [10] and that of  $\delta(4_4^+ \rightarrow 4_1^+; 942 \text{ keV})$  is not consistent with the value reported in Ref. [10].

To check the decay scheme of  $^{104}\text{Pd}$ , the  $\gamma$ - $\gamma$  coincidence spectra recorded at different angles were added up. Singles  $\gamma$ -ray energy spectra were also utilized to check or evaluate the branchings of the transitions deexciting the levels of interest.

### B. Conversion-electron measurements

Conversion-electron measurements have been performed to determine  $K$  internal conversion coefficients, to investigate  $E0$  transitions between  $0^+$  states and to evaluate  $E0$  components of transitions connecting states having the same spin. Conversion electrons were measured by means of a magnetic transport system (described in Ref. [11]) coupled with a  $5 \text{ cm}^2 \times 6 \text{ mm}$  Si(Li) detector cooled down to liquid nitrogen temperature. The energy resolution at 1 MeV was  $\sim 2 \text{ keV}$  (FWHM). The overall full energy peak efficiency of the system (at the maximum of the transmission curve) turned out to be constant (to within 2%) at a value of about 1% over the 150–1200 keV energy range and to drop to about 0.3% at 1.8 MeV. The  $\Delta p/p$  momentum acceptance of

the magnetic transport system is 18%. Gamma rays were recorded, simultaneously with electrons, by means of a HP Ge detector (placed 80 cm away from the target) having a 2.2 keV resolution at 1.3 MeV and a 25% relative efficiency. Electron and  $\gamma$ -ray spectra were corrected for dead time effects, on the basis of the real time and live time given by the acquisition system. The target, kept at a fixed position, was in thermal contact with a cold finger connected to a liquid nitrogen reservoir.

As a first step, a check of the transmission curve of the magnetic transport system was obtained by measuring the electron peak area of the 556 keV,  $2_1^+ \rightarrow 0_1^+$  transition for different magnetic field settings. Measurements have been performed by alternating a 2700 s bombarding period, followed by a 120 s waiting time to allow for the decay of short-lived isotopes, and a 2700 s measuring time. In this case, it has been possible to improve the duty ratio (as compared to the  $\gamma$ - $\gamma$  coincidence measurements), by increasing the counting rate on the Si(Li) detector since the distant geometry adopted for the germanium detector prevents overloading in the  $\gamma$  counting. Energy spectra of conversion electrons were recorded for different magnetic field settings chosen so as to span the whole energy range 150–2300 keV,

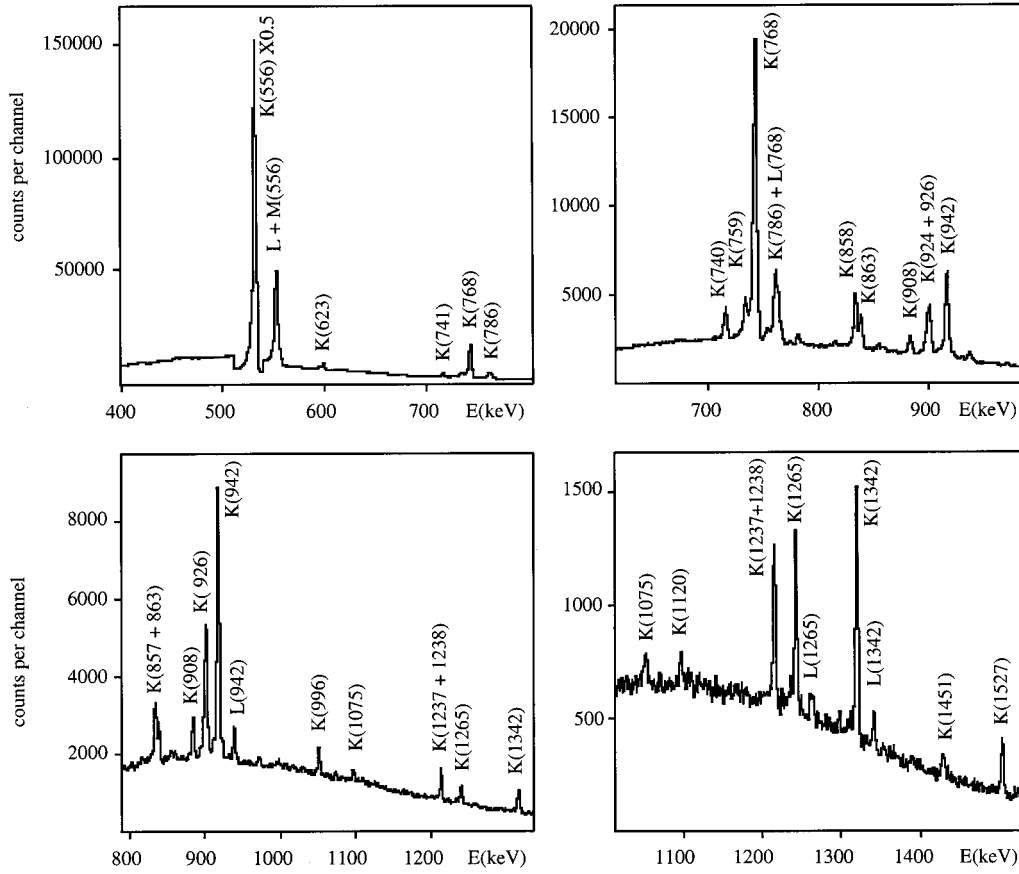


FIG. 4. Sections of the electron-energy spectra, recorded for different magnetic field settings;  $K$ -conversion and  $(L+M)$ -conversion lines are labeled by vertical labels.

with partial overlapping of the acceptance window between consecutive measurements.

The experimental values of the internal  $K$ -conversion coefficients,  $\alpha_K$ , have been deduced by using the *normalized peak-to-gamma* (NPG) method [12]. The expression for  $\alpha_K$  is given by

$$\alpha_K(E) = \frac{I_K(E)}{I_K(E_R)} \frac{\eta_e(E_R)}{\eta_e(E)} \frac{I_\gamma(E_R)}{I_\gamma(E)} \frac{\eta_\gamma(E)}{\eta_\gamma(E_R)} \alpha_K(E_R), \quad (1)$$

where  $I_K$  and  $I_\gamma$  are the peak areas in the energy spectra of electrons and  $\gamma$  rays,  $\eta_e$  and  $\eta_\gamma$  are the full-energy-peak efficiencies of  $K$  conversion and  $\gamma$ -ray lines at the energy of interest  $E$  and at the energy of the reference line  $E_R$ , while  $\alpha_K(E_R)$  is the  $K$ -conversion coefficient of the reference line of known multipolarity.

In all cases it has been possible, by a proper setting of the magnetic field, to record simultaneously both the  $K$ -conversion line of interest and the  $K$ -conversion line of a strong reference transition lying close in energy. Since the magnetic field has been set to have the maximum transmission for the line of interest, in a few cases a correction (no larger than 20%) had to be applied to take into account the reduced transmission for the reference line. Typical electron spectra, acquired for different magnetic field settings, are shown in Fig. 4.

The experimental results obtained in this work for the  $K$ -conversion coefficients are summarized in Table II. The quoted errors correspond to one standard deviation. From a comparison of these values with the theoretical ones [13] for  $E1$ ,  $M1$ , and  $E2$  multipolarities (given in the same table) it has been possible to assign the parity to several levels. In some cases information on  $\delta^2(E2/M1)$  for a mixed transition between states of known spin and parity has been obtained by comparing the experimental value of  $\alpha_K$  with the expression

$$\alpha_K = \frac{\alpha_K(M1) + \delta^2 \alpha_K(E2)}{(1 + \delta^2)}. \quad (2)$$

A few examples of the determination of  $|\delta|$  are shown in Fig. 5; the results obtained in this way are also reported in Table II, in italics.

Measurements of internal conversion electrons can also provide information on the decay properties of  $0^+$  states through the determination of intensity ratio  $q_{ifj}^2 = I_K(0_i^+ \rightarrow 0_f^+) / I_K(0_i^+ \rightarrow 2_j^+)$ . Indeed, the electric monopole strength  $\rho^2(E0; 0_i^+ \rightarrow 0_f^+)$  is related to  $q_{ifj}^2$  and to the lifetime  $\tau$  of the  $0_i^+$  level by the expression

$$\rho^2(E0; 0_i^+ \rightarrow 0_f^+) = \frac{q_{ifj}^2 \alpha_K(E2)}{\Omega_K \tau} \quad (3)$$

TABLE II. Spectroscopic data relevant to the levels in  $^{104}\text{Pd}$ , populated in the  $\text{EC-}\beta^+$  decay of  $^{104}\text{Ag}$ . Excitation energies and transition energies in the first and third columns are taken from Ref. [16], except for those given with the error, which are from the present work. Information on spin and parity given in the second and fourth columns are from Ref. [16]. Relative photon branching from each level, as determined in the present work, are given in the fifth column. Theoretical values [13] for  $K$ -internal conversion coefficients (in units of  $10^{-3}$ ) for the indicated multiplicities of the relevant transitions are listed in the sixth, seventh, and eighth columns. Those for  $M2$  multipolarity are not reported since in no case the experimental value turns out to be compatible with the theoretical  $\alpha_K(M2)$  value. The experimental values obtained in the present work are given in the ninth column while data from previous works are listed in the tenth column. The symbol  $\otimes$  in the ninth column indicates the transitions used for normalization in  $\alpha_K$  measurements via the  $NPG$  method (see text). Values or limits of  $E2/M1$  mixing ratios obtained in the present work are given in the eleventh column (here data in italics refer to absolute values of  $\delta$ ). Information on spin and parity obtained in the present work is reported in the twelfth column; the letters in the last column refer to the arguments on which such assignments are based (see text for details).

$E$ (keV)	$J_i^\pi$	$E_\gamma$ (keV)	$J_f^\pi$	%	$\alpha_K(E1)$	$\alpha_K(E2)$	$\alpha_K(M1)$	$\alpha_K^a$	$\alpha_K$	$\delta$	$J^\pi$	Comments
555.8	$2_1^+$	555.8	$0_1^+$	100		3.85		$\otimes$				
1323.6	$4_1^+$	767.7	$2_1^+$	100		1.65		$\otimes$				
1333.6	$0_2^+$	777.8	$2_1^+$	100								
1341.7	$2_2^+$	785.9	$2_1^+$	100		1.56	1.73	1.61(4)	1.79(21) <sup>b</sup>	$-32_{-170}^{+16}$		
		1341.7	$0_1^+$	78(3)		0.417		$\otimes$				
1792.9	$0_3^+$	451.1	$2_2^+$	7.5(22)								
		1237.2	$2_1^+$	100								
1794.3	$2_3^+$	460.5	$0_2^+$	2.5(6)								
		1238.0	$2_1^+$	100		0.555	0.631	0.576(39)	0.64(8) <sup>b</sup>	+0.14(9)		
		1794.0	$0_1^+$	10(1)								
1820.7	$3_1^+$	479.1	$2_2^+$	24(1)		5.88	5.49	5.39(32)	7(3) <sup>c</sup>	<1.2		
		497.8	$4_1^+$	5.7(7)		5.26	5.00	5(1)				
		1265.0	$2_1^+$	100		0.531	0.602	0.560(30)	0.61(8) <sup>b</sup>	$-15_{-23}^{+6}$		
2082.4	$4_2^+$	740.7	$2_2^+$	100								
		758.8	$4_1^+$	97(5)		1.70	1.87	1.83(6)	1.70(22) <sup>b</sup>	-0.90(14)		
		1526.6	$2_1^+$	99(4)		0.367		$\otimes$				
2139.6(2)	$0_4^+$	1583.8(2)	$2_1^+$	100								
2181.6	$4_3^+$	387.3(2)	$2_3^+$	2.3(3)								
		839.7	$2_2^+$	11(1)								
		857.9	$4_1^+$	100		1.26	1.42	1.42(9)	1.43(16) <sup>b</sup>	+0.05(10)		
		1625.8	$2_1^+$	50(3)		0.327		0.352(35)	0.27(3) <sup>b</sup>			
2193.4	( $4^+$ )	1637.5	$2_1^+$	100	0.161	0.322	0.357	<0.189			$3^-$	(b)
2244.9	$2_4^+$	1689.0	$2_1^+$	100		0.305	0.336	0.321(40)		-0.13(7)		
2249.5	$6_1^+$	926.2	$4_1^+$	100		1.05		$\otimes$				
2265.3	$4_4^+$	183.2	$4_2^+$	1.0(4)		135	63.5	68(6)		<0.4		
		444.5	$3_1^+$	6.6(6)		7.34	6.59	7.29(27)	11(2) <sup>c</sup>	>1.2		
		923.3	$2_2^+$	27(2)		1.06	1.20	1.02(8)				
		941.7	$4_1^+$	100		1.01	1.15	1.04(6)	1.18(14) <sup>b</sup>	-3.5(8)		
		1708.0	$2_1^+$	0.70(8)								
2276.5	$1^+, 2^+$	483.5(4)	$0_3^+$	8(1)							$1^+$	(a)
		934.6	$2_2^+$	22(3)						-0.14(7)		
		942.0(5)	$0_2^+$	24(11)								
		1720.8	$2_1^+$	75(3)		0.295	0.324	0.305(52)	0.45(10) <sup>b</sup>	-0.16(3)		
		2276.7	$0_1^+$	100								
2298.9	$4^-$	116.3	$4_3^+$	54(30)								
		215.6	$4_2^+$	83(17)								
		974.2	$4_1^+$	100								
2337.9	$1^+, 2^+$	996.1	$2_2^+$	20(2)						-3.1(9)	$2^+$	(a)
		1781.8	$2_1^+$	100								
		2338.0	$0_1^+$	39(4)								
2444.5	$4^+, 5^+, 6^+$	179.3	$4_4^+$	36(6)		145	67.3	68.6(35)		<0.25	$5^+$	(a)
		263.2	$4_3^+$	26(3)		39.1	24.5	30(3)	54(16) <sup>c</sup>	0.8(4)		
		362.3	$4_2^+$	50(7)		13.8	10.9	9.7(8)	13(3) <sup>c</sup>	<i>MI</i>		

TABLE II. (Continued).

$E$ (keV)	$J_i^\pi$	$E_\gamma$ (keV)	$J_f^\pi$	%	$\alpha_K(E1)$	$\alpha_K(E2)$	$\alpha_K(M1)$	$\alpha_K^a$	$\alpha_K$	$\delta$	$J^\pi$	Comments
2456.6	(1,2,3)	623.2	$3_1^+$	100		2.82	2.94	2.74(16)				
		1120.5	$4_1^+$	39(6)		0.687	0.785	0.73(13)		-0.35(15)		
		1133.1	$4_1^+$	83(13)	0.299	0.670	0.766	0.77(39)		or $-3.9_{-4.7}^{+1.7}$	3	(c),(d),(e)
		1900.9	$2_1^+$	100	0.128	0.247	0.269	0.41(30)				
2521.4	$2^+$	1179.3	$2_2^+$	100								
		1965.6	$2_1^+$	67(14)								
2533.4	(1,2,3)	1191.5	$2_2^+$	17(3)							$2^+$	(a)(b)
		1977.5	$2_1^+$	100	0.121	0.230	0.249	0.22(5)		-5(2)		
2570.9(2)		1247.3(2)	$4_1^+$	100	0.251	0.547	0.621	0.522(96)	1.09(47) <sup>b</sup>	-0.80(7)	$4^+$	(a),(b),(c)
2572.6(2)		1231.0(2)	$2_2^+$	100	0.258	0.562	0.639	0.86(20)			$1^+, 2^+, 3^+$	(b),(c)
		2016.8(2)	$2_1^+$	64(14)								
2613.4	$2^+, 3^+$	1271.7	$2_2^+$	100							$2^+$	(e)
		2613.4	$0_1^+$	19(4)								
2622.2	(1,2,3)	1297.8	$4_1^+$	100	0.234	0.503	0.570	0.50(10)			$2^+, 3^+$	(b),(c)
2642.6	$4^+$	1300.0	$2_2^+$	15(3)								
2677.8	$4^+$	1318.2	$4_1^+$	100	0.228	0.488	0.522	0.55(14)				
		1354.3	$4_1^+$	100								
2695.0	$2^+$	2139.2	$2_1^+$	100						-0.11(6)		
2714.8	(4,5,6)	1372.6	$2_2^+$	100	0.211	0.444	0.500	0.38(20)			$3^-, 4^+$	(b),(c)
		2158.9	$2_1^+$	25(10)								
2771.5		2215.6	$2_1^+$	100								
2774.5	$4^+$	1451.2	$4_1^+$	100	0.194	0.404	0.452	0.483(64)		$-0.9_{-0.3}^{+1.0}$		
		2218.3	$2_1^+$	8(2)	0.101	0.186	0.199	0.205(78)				
2800.5	$4^+$	2244.6	$2_1^+$	100								
2803.7(2)		1480.1(2)	$4_1^+$	100	0.188	0.389	0.434	0.35(9)			$4^+, 5^+, 6^+$	(b),(c)
2868.4(7)		618.6(2)	$6_1^+$	100	1.03	2.89	3.00	3.37(27)			$(4)^+$	(a),(b)
		1545.2(3)	$4_1^+$	80(5)	0.175	0.358	0.399	0.39(15)		-0.90(13)		
2875.2	(4,5,6)	1551.6	$4_1^+$	100	0.174	0.356	0.395	0.40(16)			$4, 5, 6^+$	(b),(c),(d)
2918.3	$(1, 2, 3)^+$	1576.7(2)	$2_2^+$	7(1)							$1^+, 2^+$	(c),(d),(e)
		1584.3(3)	$0_2^+$	10(5)								
2924.2	$(4, 5, 6)^+$	2362.4	$2_1^+$	100								
		659.3	$4_4^+$	39(4)		2.43	2.58	2.30(35)			$4^+, 5^+$	(a)
		742.3(3)	$4_3^+$	20(4)								
2975.5	(1,2,3)	1600.0	$4_1^+$	100		0.336	0.372	0.365(41)				
		699.0(4)	$1_1^+$	6(1)							$2, 3$	(a)
		1154.4(2)	$3_1^+$	10(2)								
2993.6	$4^+$	2419.6	$2_1^+$	100								
		1652.1	$2_2^+$	100							$1, 2, 3$	(c),(d)
3008.3	$(1, 2^+)$	2437.3	$2_1^+$	74(37)								
		2452.2	$2_1^+$	100								
3034.0	$(1, 2^+)$	2478.3(2)	$2_1^+$	36(1)							$1, 2$	(c),(d),(e)
		3034.0	$0_1^+$	100								
3078.5	$2^+, 3^+$	1283.7(2)	$2_3^+$	5(4)								
		2522.7	$2_1^+$	100								
3105.0	$4^+$	806.3(2)	$4^-$	9.9(9)	0.582	1.47	1.63	0.63(4)				
		1022.9	$4_2^+$	20(2)		0.840	0.960	0.82(15)	0.70(13) <sup>b</sup>			
		1283.9	$3_1^+$	19(4)		0.514	0.583	0.500(98)				
		1763.1	$2_2^+$	18.9(5)								
		1781.8	$4_1^+$	100							-1.4(3)	
3112.8	$5^+, 6^+$	2549.0	$2_1^+$	2.2(4)						or $+0.24(10)$		
		847.5(5)	$4_4^+$	4(1)								
		863.0	$6_1^+$	100		1.24	1.40	1.31(10)	1.69(19) <sup>b</sup>			

TABLE II. (*Continued*).

$E$ (keV)	$J_i^\pi$	$E_\gamma$ (keV)	$J_f^\pi$	%	$\alpha_K(E1)$	$\alpha_K(E2)$	$\alpha_K(M1)$	$\alpha_K^a$	$\alpha_K$	$\delta$	$J^\pi$	Comments
3136.9	$4^+$	1031.0(2)	$4_2^+$	5.0(7)								
		1789.2(3)	$4_1^+$	3.2(4)								
		872.0(2)	$4_4^+$	26(6)		1.21	1.37	1.26(33)				
		955.3	$4_3^+$	52(8)		0.982	1.12	1.05(26)				
		1813.7	$4_1^+$	100		0.269	0.294	0.309(80)		-0.5(4)		
3157.9	$4^+$	2582.3	$2_1^+$	8(1)								
		289.0(6)	$(4)_1^+$	20(5)		29.5	19.8	19(1)		<1.5	$5^+, 6^+$	(a),(b)
		892.6	$4_4^+$	13(2)		1.15	1.30	1.01(15)		>4		
		908.0	$6_1^+$	100		1.10	1.25	1.18(3)	1.29(15) <sup>b</sup>	$0.9_{-0.3}^{+0.5}$		
		1075.3	$4_2^+$	55(8)		0.752	0.860	0.770(11)	1.00(13) <sup>b</sup>	$2.2_{-0.6}^{+1.6}$		
3182.6(3)		1835.0	$4_1^+$	3.3(6)								
		1388.3(3)	$2_3^+$	17(1)							2,3	(a)
		1841.0(4)	$2_2^+$	7.3(5)								
3213.5	$1^+, 2^+, 3^+$	2627.1(3)	$2_1^+$	100								
		1420.5(2)	$0_3^+$	7(1)							2 <sup>+</sup>	(e)
		1880.1(3)	$0_2^+$	2.5(2)								
		1889.9(1)	$4_1^+$	28(2)		0.250	0.272	0.30(10)				
		2657.5	$2_1^+$	23(3)								
3285.4	$4^+$	3213.6	$0_1^+$	100								
		1490.8(2)	$2_3^+$	11.5(9)							1,2 <sup>+</sup>	(e)
		2729.5	$2_1^+$	100								
3309.6	4,5,6	3285.6(3)	$0_1^+$	3.5(5)								
		1986.0	$4_1^+$	100						-1.4(6)	4	(a)
3333.8	$(3^-, 4^-)$	2777.9	$2_1^+$	100								
3408.0	$1^+, 2^+, 3^+$	2065.9	$2_2^+$	15(1)							1 <sup>+</sup> , 2 <sup>+</sup>	(e)
		2852.5	$2_1^+$	19(1)								
		3407.8	$0_1^+$	100								
3474.4	$4^+$	2918.8	$2_1^+$	100							1,2 <sup>+</sup>	(c),(d),(e)
		3473.9	$0_1^+$	52(5)								
3608.5		1343.0(8)	$4_4^+$	100(24)							4 <sup>+</sup>	(c),(d),(e)
		1787.6(3)	$3_1^+$	38(5)								
		2267.3(5)	$2_2^+$	43(4)								
		2284.1	$4_1^+$	17(4)								

<sup>a</sup>Present work.

<sup>b</sup>Reference [17].

<sup>c</sup>Reference [22].

where  $\Omega_K$  is the electronic factor for the  $K$  conversion of the  $E0$  transition (tabulated, e.g., in Ref. [14]) and  $\alpha_K$  is the  $K$ -internal conversion coefficient of the  $0_i^+ \rightarrow 2_j^+$  transition. If the lifetime of the level is unknown, one can still deduce the ratio  $X_{ifj}$  of the electric monopole  $B(E0; 0_i^+ \rightarrow 0_f^+)$  to the electric quadrupole  $B(E2; 0_i^+ \rightarrow 2_j^+)$  reduced transition probabilities via the expression [15]

$$X_{ifj} = 2.56 \times 10^9 A^{4/3} E_\gamma^5 [\text{MeV}] \frac{\alpha_K(E2) q_{ifj}^2}{\Omega_K [s^{-1}]} \quad (4)$$

In the analysis we have considered the decay of the  $0_2^+$  and  $0_3^+$  states. To deduce  $q_{ifj}^2$  each electron energy spectrum was normalized to the intensity of the simultaneously recorded  $0_i^+ \rightarrow 2_j^+$   $\gamma$  transition since the intensities of the elec-

tron lines were derived from spectra recorded at different times. The analysis of the  $0_3^+ \rightarrow 0_1^+$   $K$ -electron line (1768.5 keV) was made difficult by the presence in the electron spectrum of the 1769.9 keV line from the  $K$  conversion of the  $2_3^+ \rightarrow 0_1^+$  transition. As a consequence, only an upper limit (95% confidence level) could be given for  $q_{311}^2$ . The ratios  $q_{ifj}^2$  for the relevant transitions turn out to be

$$q_{211}^2 = 0.20(3) \quad \text{and} \quad q_{311}^2 \leq 0.07$$

and the corresponding  $X_{ifj}$  values are

$$X_{211} = 0.029(4) \quad \text{and} \quad X_{311} \leq 0.02.$$

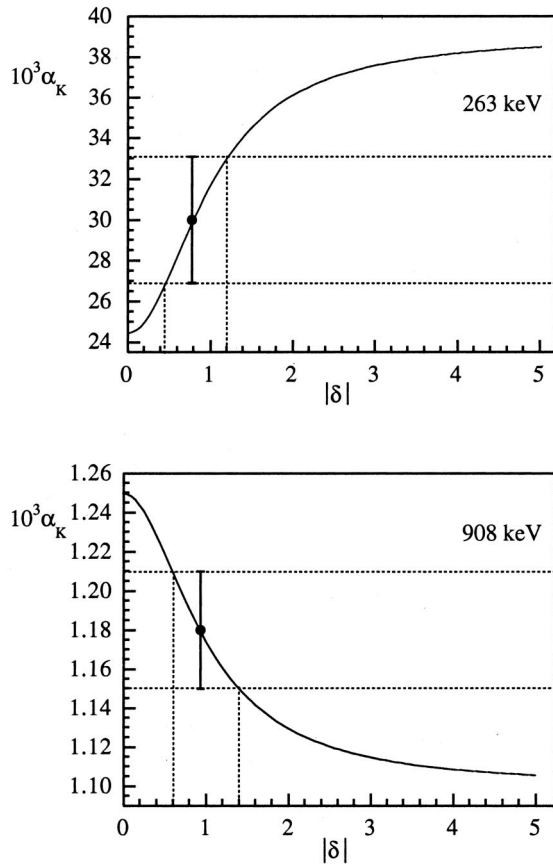


FIG. 5. The calculated curves of  $\alpha_K$  as a function of  $|\delta|$ , for the 263 keV (from the 2444 keV level) and 908 keV (from the 3158 keV level) transitions are compared with the experimental value of  $\alpha_K$ . The error bar corresponds to one standard deviation.

From the known value [16] of the lifetime [ $\tau=7.5(7)$  ps] of the  $0_2^+$  level we derived the value of the electric monopole strength

$$\rho^2(E0;0_2^+ \rightarrow 0_1^+) = 0.011(2).$$

The value of  $q_{211}^2$  is larger than that [0.034(5)] reported in Ref. [17] and the value of  $X_{211}$  is larger than that [0.012(4)] given in Ref. [18]. We have no explanation for such different values. We only note that the authors of Ref. [17] find a quite different value of  $q_{211}^2$  in  $^{106}\text{Pd}$  [0.24(6)], close to our value for  $q_{211}^2$  in  $^{104}\text{Pd}$ , and that the comparison of  $K$ -conversion coefficients (where possible) between our values and those reported in Ref. [17] (see Table II) shows no discrepancy.

Information on the  $E0$  component of a transition between two states of the same  $J$  ( $\neq 0$ ) and parity can be obtained by comparing the experimental value of  $\alpha_K$  with the theoretical value corresponding to a transition having  $E0$ ,  $M1$ , and  $E2$  multipole components

$$\alpha_K = \frac{\alpha_K(M1) + (1 + q_{iff}^2) \delta^2 \alpha_K(E2)}{(1 + \delta^2)}. \quad (5)$$

Notice that, compared to Eq. (2), there is the additional factor  $(1 + q_{iff}^2)$  where  $q_{iff}^2$  is the intensity ratio of  $K$ -conversion electrons for the monopole and quadrupole components of the  $J_i \rightarrow J_f$  transition. If  $\delta^2$  is independently known, it may be possible to deduce  $q_{iff}^2$  and then  $X_{iff}$ ; when the lifetime of the level is also known one can deduce  $\rho^2(E0;J_i \rightarrow J_f)$ .

By using in Eq. (5) the values we have measured for  $\alpha_K$  and  $\delta$  and the known lifetimes of the  $2_2^+$  and  $4_2^+$  levels [16], the value or the upper limit (95% confidence level) of  $X$  and  $\rho$  for the indicated transitions has been obtained:

$$X(E0;2_2^+ \rightarrow 2_1^+) = 0.086(69),$$

$$\rho^2(E0;2_2^+ \rightarrow 2_1^+) = 0.010(8),$$

$$X(E0;4_2^+ \rightarrow 4_1^+) \leq 0.05, \quad \rho^2(E0;4_2^+ \rightarrow 4_1^+) < 0.09,$$

$$X(E0;4_3^+ \rightarrow 4_1^+) \leq 25,$$

$$X(E0;4_4^+ \rightarrow 4_1^+) \leq 0.06.$$

### C. Decay scheme

The new spectroscopic information on branching ratios,  $K$ -conversion coefficients, mixing ratios, and spin parity in  $^{104}\text{Pd}$  is summarized in Table II together with previously available experimental data from studies of the EC  $\beta^+$  decay of  $^{104}\text{Ag}$ . Figures 6 and 7 show the level scheme based on the results of the present work.

For several levels new spin-parity assignments, reported in the last column of Table II, have been obtained. They were deduced on the basis of the following points.

- The results of angular correlation measurements.
- The comparison between theoretical and experimental values of  $K$ -conversion coefficients.

(c) The assessment whether each level of interest is populated from the  $5^+$  and/or from the  $2^+$  state of  $^{104}\text{Ag}$ . This information has been obtained by checking, as a function of time, the intensity ratio of the deexciting  $\gamma$  rays to a reference  $\gamma$ -ray deexciting a level that is known to be strongly populated only by either the  $5^+$  or the  $2^+$  level of  $^{104}\text{Ag}$ .

(d) The values of  $\log ft$  (from the present work and Ref. [16]). In the calculation of  $\log ft$  the usual practice [16] of utilizing the integral Fermi function (with Coulomb corrections) for allowed transitions [19] has been adopted. Restriction on the spin of the levels of the daughter nucleus have been derived on the basis of the distribution of the available experimental  $\log ft$  values summarized in Ref. [20].

(e) The assumption that in the decay of a given level an  $E3$  or  $M3$  transition would have a negligible intensity with respect to that of  $E1$ ,  $M1$ ,  $E2$  transitions of similar energy.

Compared to the decay scheme reported in Ref. [16] we find a number of differences that are listed below:

The 2140 keV,  $0^+$  level, observed in light particle reactions [16] and not reported in previous studies of the EC- $\beta^+$  decay of  $^{104}\text{Ag}$ , turns out to be very weakly populated (0.03%) in the decay of the  $2^+$  state of  $^{104}\text{Ag}$ .



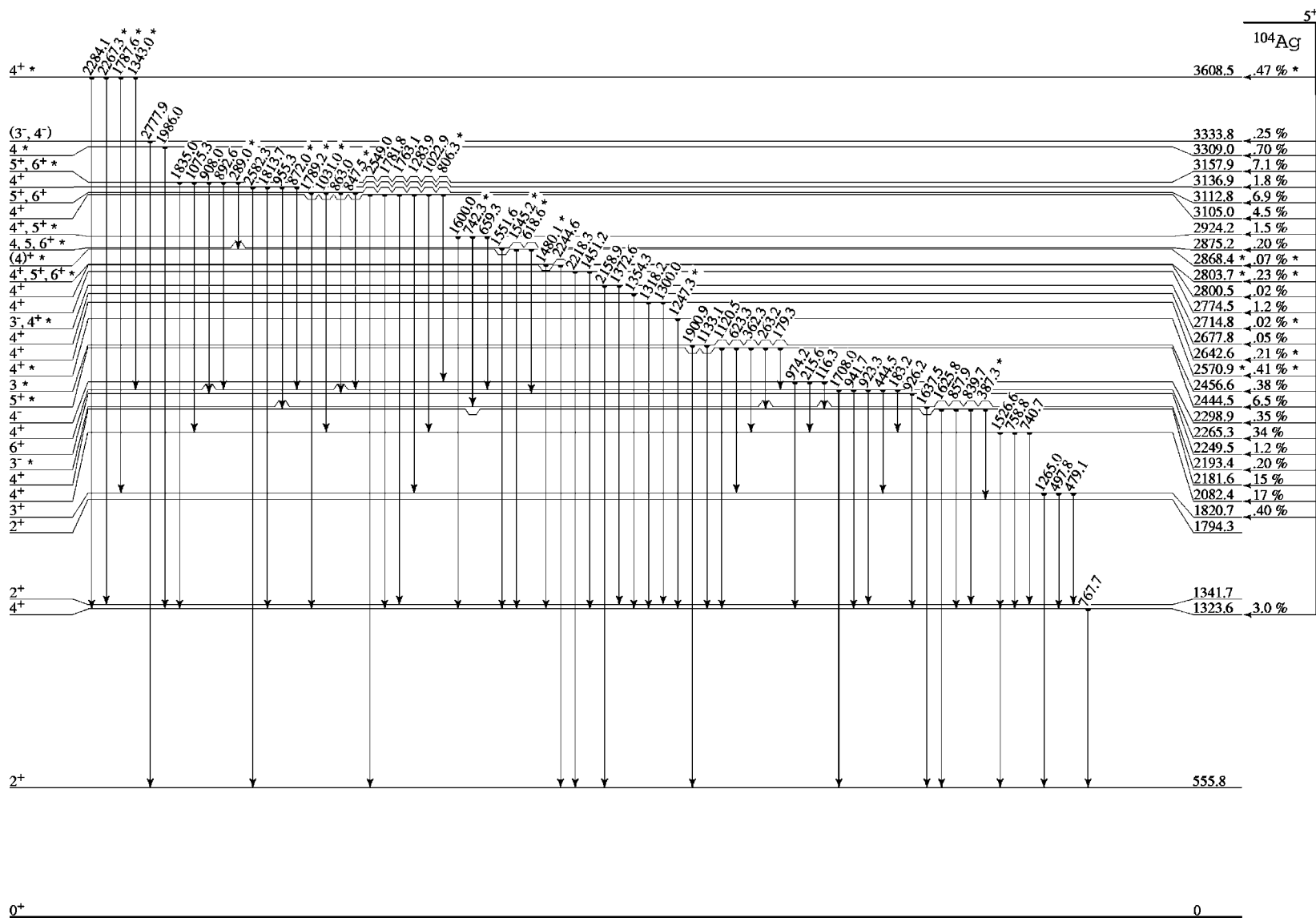


FIG. 7. As in Fig. 6, for the states directly populated in the EC  $\beta^+$  decay of the  $J^\pi = 5^+$  level of  $^{104}\text{Ag}$ .

Four new levels at 2573, 2804, 2868, and 3183 keV have been identified by analyzing the coincidence data. In particular, we establish a close doublet of levels at an energy around 2570 keV, where Ref. [16] reports just a single level at 2570.3(4) keV of spin parity  $4^+$ , populated from both the  $2^+$  (1.2%) and  $5^+$  (0.75%) states of  $^{104}\text{Ag}$ . For this level, that we found to be populated only from the  $5^+$  state of  $^{104}\text{Ag}$  (0.41%,  $\log ft=6.8$ ), we measure an energy of 2570.9(2) keV and assign  $J=4$  from angular correlation measurements. The other member of the doublet at 2572.6 keV was found to be populated (0.40%,  $\log ft=6.5$ ) only by the  $2^+$  state of  $^{104}\text{Ag}$  and to deexcite to the  $2_1^+$  and  $2_2^+$  levels.

The 2804 and 2868 keV levels are found to be fed only in the decay of the  $5^+$  state of  $^{104}\text{Ag}$ , with an intensity 0.23% and 0.07% and  $\log ft=6.9$  and 7.4, respectively.

The 3183 keV level is populated (1.0%,  $\log ft=6.0$ ) only in the decay of the  $2^+$  state of  $^{104}\text{Ag}$ .

In the evaluations of the feedings of these levels (as well as those of the levels mentioned below) the known feedings of the 2875 keV and 2695 keV levels populated only in the decay of the  $5^+$  and of the  $2^+$  state of  $^{104}\text{Ag}$ , respectively, have been utilized as reference values and no renormalization has been performed.

The existence of the level at 3608 keV, tentatively reported in Refs. [16,21] is confirmed by our data. Indeed, beside the 2284 keV transition already reported in Ref. [16], three new transitions from this level to the  $4_4^+$ ,  $3_1^+$ , and  $2_2^+$  levels have been identified. The level is only populated (0.47%,  $\log ft=5.9$ ) in the decay of the  $5^+$  state of  $^{104}\text{Ag}$ . The presence of a transition to the  $2_2^+$  level in competition with a transition of similar energy to the  $4_1^+$  level allows one to safely exclude the negative parity. The decay mode of this level then restricts its spin value to 4.

From the analysis of the coincidence spectra the following levels, reported in Ref. [16], have been canceled from the decay scheme.

(1) 1941 keV level. We found no evidence for a 617.6 keV line (the only one reported as deexciting this level) in coincidence with the  $4_1^+ \rightarrow 2_1^+$  transition, whereas we assign a 618.6 keV transition, seen in several gated spectra (e.g., in the  $6_1^+ \rightarrow 4_1^+$  gate) to the newly found level at 2868 keV.

(2) 2479 and 2627 keV levels. For both levels a partial decay to the  $0_1^+$  level has been reported in Ref. [16], whereas we found the 2478.3 and 2627.1 keV transitions to be in coincidence with the  $2_1^+ \rightarrow 0_1^+$  transition. Moreover, we cannot confirm the decay of these levels to the  $2_1^+$  level since no evidence was found for the 1924 and 2070 keV  $\gamma$  lines either in the gated or in the singles spectra. On the other hand, the sums (2478.3 + 555.6) keV and (2627.1 + 555.6) keV match, within the experimental uncertainty, the energy of the levels at 3034.0(5) keV, reported in Ref. [16], and that of the newly found level at 3182.6(3) keV, respectively.

(3) 3590 keV level. The 2267 keV transition, reported in Ref. [16] as the only one deexciting this level, turns out to be in coincidence with the  $2_2^+ \rightarrow 2_1^+$  keV transition and was assigned to the 3608.5 keV level (see above).

We did not find any evidence for the feeding of the levels at 1999, 2492, 2760, 2767, 2810, 2960, 3098, 3113.3,

3115.6, 3116.3, 3193, 3280, 4009, and 4030 keV. In fact none of the deexciting transitions (which, assuming the intensity reported in Ref. [16], should have been far above the sensitivity threshold of our apparatus) is observed either in the singles or coincidence  $\gamma$  spectra.

For a few levels the feeding observed in the present work is quite different from that reported in Ref. [16]: level at 2521 keV, 0.05% feeding instead of 0.21%; level at 2622 keV, 0.03% feeding instead of 0.9%; level at 2613 keV, reported as populated 0.06% in the decay of the  $5^+$  state of  $^{104}\text{Ag}$  is found to be fed (0.27%) only in the decay of the  $2^+$  state; level at 2642, reported to be populated 0.075% in the decay of the  $2^+$  state of  $^{104}\text{Ag}$  is found to be fed (0.21%) only in the decay of the  $5^+$  state; level at 2715 keV, reported to be populated from both the  $2^+$  and  $5^+$  state of  $^{104}\text{Ag}$  is found to be fed (0.02%) only in the decay of the  $5^+$  state of  $^{104}\text{Ag}$ .

As to the  $\gamma$  branching ratios for the individual levels, there is a general satisfactory agreement between our data and those of previous works, apart from the obvious differences due to the new transitions identified and/or differently placed in the present work. However, there are also some noticeable discrepancies on which we comment hereafter.

(i) The intensity of the 498 keV,  $3_1^+ \rightarrow 4_1^+$  transition with respect to the 1265 keV transition from the 1820 keV level was measured to be a factor 13 lower than that reported in Ref. [16].

(ii) The intensity of the 179 keV transition from the 2444 keV level relative to the 623 keV transition is found to be about a factor 18 larger than that reported in Ref. [16]; moreover, we note that the 1890 keV transition, previously reported to deexcite the 2444 keV level to the  $2_1^+$  state (which is incompatible with the present assignment  $J=5$  to the former level), turns out to be in coincidence with the  $4_1^+ \rightarrow 2_1^+$  transition and is therefore assigned to the decay of the 3213 keV level to the  $4_1^+$  level.

(iii) No evidence has been found for transitions from the 2298 and 2643 keV levels to the  $2_1^+$  state, from the 2245 and 3334 keV levels to the  $2_2^+$  state, from the 2715 keV level to the  $0_2^+$ ,  $4_1^+$  states, from the 2994 keV level to the  $4_1^+$  state, from the 3008 keV level to the  $0_1^+$  state.

In five cases we disagree with the spin-parity reported in Ref. [16].

2193 keV level. On the basis of the present upper limit for the  $\alpha_K$  of the 1638 keV transition, we agree with the  $3^-$  assignment given in Refs. [21,18], whereas a  $J^\pi=4^+$  is suggested in Ref. [16].

2994 keV level. It is populated only from the  $2^+$  state of  $^{104}\text{Ag}$  (0.05% instead of 0.23% as given in Ref. [16]); the computed  $\log ft$  is 7.1, so that the possible spin values are restricted to 1, 2, or 3, incompatible with the previous  $J=4$  assignment.

3158 keV level. The previous spin assignment  $J=4$  is ruled out by the results of the angular correlation measurements (see Table I) as well as by the large  $M1$  component in the 908 keV transition to the  $6_1^+$  level, as implied by the measured value of  $|\delta|$ .

*3285 and 3474 keV levels.* The presence of the deexciting transition to the  $0_1^+$  state, together with the fact that they are populated only in the EC- $\beta^+$  decay of the  $2^+$  state in  $^{104}\text{Ag}$  (as checked in this work), rules out the previous  $4^+$  assignment and restricts the spin value to 1 or 2.

### III. CONCLUSIONS

To summarize,  $\gamma$ - $\gamma$  coincidence and angular correlation measurements as well as  $\alpha_K$  measurements have been performed in  $^{104}\text{Pd}$  populated in the EC- $\beta^+$  decay of  $^{104}\text{Ag}$ . Major changes of the excitation-energy pattern with respect to that reported in the literature [16] proved to be necessary, and an improved knowledge of the decay properties of several levels (branching ratios and  $E2/M1$  mixing ratios) has

been gained. Information on  $E0$  transitions between  $0^+$  states and between states having  $J_i=J_f\neq 0$  has also been obtained.

The new experimental information obtained in the present work on spin-parity and decay properties of levels in  $^{104}\text{Pd}$  will be exploited in a detailed phenomenological study of this nucleus. This analysis, performed in the framework of the IBA-2 model, will focus on the identification of mixed-symmetry states and will be presented in a forthcoming paper.

### ACKNOWLEDGMENTS

We are indebted to M. Ottanelli and A. Pecchioli for their skillful and continuous technical assistance.

- 
- [1] F. Iachello and A. Arima, *The Interacting Boson Model* (Cambridge University Press, Cambridge, England, 1987).
- [2] F. Pan and J.P. Draayer, Nucl. Phys. **A636**, 156 (1998).
- [3] K.H. Kim, A. Gelberg, T. Mizusaki, T. Otsuka, and P. von Brentano, Nucl. Phys. **A604**, 163 (1996).
- [4] A. Giannatiempo, A. Nannini, and P. Sona, Phys. Rev. C **58**, 3316 (1998).
- [5] A. Giannatiempo, A. Nannini, and P. Sona, Phys. Rev. C **58**, 3335 (1998).
- [6] A. Arima, T. Otsuka, F. Iachello, and I. Talmi, Phys. Lett. **66B**, 205 (1977).
- [7] T. Otsuka, A. Arima, F. Iachello, and I. Talmi, Phys. Lett. **76B**, 139 (1978).
- [8] K.S. Krane, At. Data Nucl. Data Tables **16**, 383 (1975).
- [9] K.S. Krane, Nucl. Instrum. Methods **21**, 209 (1963).
- [10] J.A. Grau, L.E. Samuelson, F.A. Rickey, P.C. Simms, and G.J. Smith, Phys. Rev. C **14**, 2297 (1976).
- [11] P. Del Carmine, A. Giannatiempo, A. Nannini, A. Perego, A. Pecchioli, and M. Ottanelli, Report No. DFF311-6/98, Università degli Studi di Firenze, 1998.
- [12] J.H. Hamilton, in *The Electromagnetic Interaction in Nuclear Spectroscopy*, edited by W.D. Hamilton (North-Holland, Amsterdam, 1975), p. 451.
- [13] F. Rösler, H.M. Fries, K. Alder, and H.C. Pauli, At. Data Nucl. Data Tables **21**, 91 (1978).
- [14] D.A. Bell, C.E. Avelledo, M.G. Davidson, and J.P. Davidson, Can. J. Phys. **48**, 2542 (1970).
- [15] A.V. Alduschenkov and N.A. Voinova, Nucl. Data Tables **11**, 299 (1973).
- [16] R.B. Firestone, in *Table of Isotopes*, edited by V.S. Shirley (Wiley, New York, 1996).
- [17] K. Farzine, H. Hardenberg, H. Möllmann, K. Uebelgünn, and H. von Buttler, Z. Phys. A **326**, 401 (1987).
- [18] M. Luontama, R. Julin, J. Kantele, A. Passoja, W. Trzaska, A. Bäcklin, N.G. Jonsson, and L. Westerberg, Z. Phys. A **324**, 317 (1986).
- [19] N.B. Gove and M.J. Martin, Nucl. Data Tables **10**, 206 (1971).
- [20] B. Singh, J.L. Rodriguez, S.S.M. Wong, and J.K. Tuli, Nucl. Data Sheets **84**, 487 (1998).
- [21] K. Müller, K. Farzine, and H. von Buttler, Z. Phys. A **284**, 189 (1978).
- [22] H. Nutley and J.B. Gerhart, Phys. Rev. **120**, 1815 (1960).